agriculture

MDPI

Article

Evaluation on the Performance of Airflow Distribution Device of Pneumatic Seeder for Rapeseed through CFD Simulations

Zhaodong Li [1,2], Heng Zhang [1], Rui Xie [1], Xin Gu [1], Juanhui Du [1] and Yongxin Chen [1,2,*]

[1] School of Engineering, Anhui Agricultural University, Hefei 230036, China
[2] Laboratory of Engineering of Intelligent Agricultural Machinery Equipment, Hefei 230036, China
* Correspondence: cyx_zcz@sohu.com

Abstract: The seeding performance of a pneumatic seed-metering equipment for rapeseed has a significant bearing on the sowing effect. When the negative pressure falls abruptly, the pneumatic system experiences a significant loss of negative pressure. This will prevent rapeseed from being entirely absorbed by the seed plate, resulting in inconsistent seeding quantities along each row. In this study, CFD simulations were used to analyze the airflow field affecting the airflow transmission of an airflow distribution device. The essential structural characteristics of a conical cylinder conical-arranged kind of airflow distribution device were found, and the causes of negative pressure loss were analyzed from the standpoint of fluid kinematics. The optimal structural type of airflow distribution device was determined using fluid simulation. In addition, an orthogonal examination of the ideal type's essential structural characteristics was conducted to minimize negative pressure loss during airflow transmission. Then, the influence of the negative pressure loss rate of the airflow distribution device on the variation coefficient of seeding quantity in each row of the seed-metering device was investigated using a bench test involving three factors: seed plate rotational speed, working negative pressure, and structure type. It was discovered that three parameters have highly substantial impacts on the negative pressure loss rate and the variation coefficient of seeding quantity in each row, and that the negative pressure loss rate correlates positively with the variation coefficient of the seeding quantity in each row. When negative pressure fell to 500 Pa, the negative pressure loss rate of the optimal structure type and the variation coefficient of seeding amount in each row of the seed-metering device fell by 6.25% and 3.45%, respectively. Field experiments reveal that the negative pressure loss rate of an airflow distribution device was below 20% and that the variation coefficient of seeding amount in each row of seed-metering devices was below 3.5%. The results can be used to analyze the construction of the pneumatic system and enhance the performance of the seed-metering equipment.

Keywords: rapeseed; airflow distribution device; pneumatic seeder; optimization; negative pressure loss

Citation: Li, Z.; Zhang, H.; Xie, R.; Gu, X.; Du, J.; Chen, Y. Evaluation on the Performance of Airflow Distribution Device of Pneumatic Seeder for Rapeseed through CFD Simulations. *Agriculture* **2022**, *12*, 1781. https://doi.org/10.3390/agriculture12111781

Academic Editor: Jin He

Received: 13 September 2022
Accepted: 20 October 2022
Published: 26 October 2022

1. Introduction

China's main oil crop, rapeseed, plays a crucial role in production [1]. Presently, pneumatic seeding technology is most commonly used for mechanized planting of rapeseed because it is well-suited to small-grain seeds, does not easily harm the seeds, and performs well under high-speed sowing conditions [2].

The pneumatic system is a crucial component of the pneumatic seeder for rapeseed [3]. The airflow distribution device under negative pressure is the key component of the pneumatic system. Its primary function is to distribute the negative pressure crated by the air pump evenly and with little loss into the chamber of each seed-metering device. When negative pressure falls abruptly, its low loss can enhance the consistency of plant spacing in each sowing row and assure the rate of rapeseed emergence. Pneumatic systems have been the subject of substantial investigation by both domestic and foreign academics. Li et al. [4] conducted simulation research on the airflow field in the positive and negative pressure zones of a pneumatic seeder for rapeseed; Li et al. [5] used the CFD simulation approach

to analyze the internal airflow field of the seed-metering device. Lei et al. [6,7] conducted extensive research on centralized air-assisted seed-metering machines for rapeseed and wheat, optimizing the structure through the distribution of airflow velocity and pressure to effectively improve the distribution performance. Ahmad et al. [8] studied the sowing uniformity of pneumatic maize planters at different seedbed preparation levels and machine travel speeds; Liu et al. [9] analyzed and studied the related factors that affect the pressure loss of an evenly-sowing device for wheat; and Yatskul et al. [10,11] studied the distribution heads of pneumatic planters. Yin et al. [12] analyzed the impacts of airflow velocity and material transit speed on the precision of seed distribution, focusing on the pneumatic system of corn planters. They created a uniform and low-loss airflow distribution device to address the issues of uneven airflow distribution and excessive negative pressure loss. There has been extensive research on the simulation of pneumatic systems in the seeding process in the aforementioned studies; it demonstrates that CFD simulation is a trustworthy method for studying airflow fields. In the field work of a pneumatic planter, the planter's power output shaft provides the air pressure. Starting, rotating, and stopping the planter precipitously reduced the air pressure, making it difficult to maintain a consistent air pressure which severely affected the sowing quality. Therefore, the loss of air pressure was minimized as much as possible during the transfer of wind pressure to increase the negative working pressure of the meter device. However, there have been few studies on the design and structural optimization of airflow distribution devices, the cause of negative pressure loss, and the effect of seed-metering devices on seeding performance.

In a prior constructed study, our group designed a cylindrical, circularly structured airflow distribution device and simulated the airflow field within it. The airflow distribution device was originally optimized, and a circularly arranged conical cylinder was built based on the literature [13]. Then, using fluid modelling, the negative pressure loss of two types of airflow distribution devices was examined. However, the performance of airflow distribution devices has a significant impact on the performance of pneumatic seed-metering devices. In the prior study, the team did not investigate the performance of airflow distribution devices; therefore, the structural kinds and characteristics required additional optimization and improvement.

In this paper, a conical cylinder airflow distribution device with a conical arrangement is constructed. Then, using Fluent, we simulated the airflow field for three types, analyzed the causes of negative pressure loss, and determined the ideal structural type of airflow distribution device. In addition, the characteristics of the best structural kind of airflow distribution device, the selected model, were adjusted. We conducted bench comparison tests and field testing to validate the simulation's correctness. These findings will assist in enhancing the performance of seed-metering systems for rapeseed.

2. Analysis of the Working Principle and Parameters

2.1. Structure of Pneumatic Seeder

The pneumatic system, a crucial component of the pneumatic seeder for rapeseed (Figure 1), consisted of an air pump, positive and negative pressure airflow supply hoses, an airflow distribution device, a seed-metering device for rapeseed, a seed guiding tube, and other components.

The negative pressure airflow distribution device is the core working part of the pneumatic system, which is composed of an outlet, four inlets, and an airflow guiding chamber. The airflow-guiding chamber is a conical cylinder, which includes two conical cylinders: the upper conical cylinder is connected to four inlets, the lower conical cylinder is connected to the outlet, and the four inlets are arranged conically. Furthermore, a small cone is excavated inside to separate airflow more evenly.

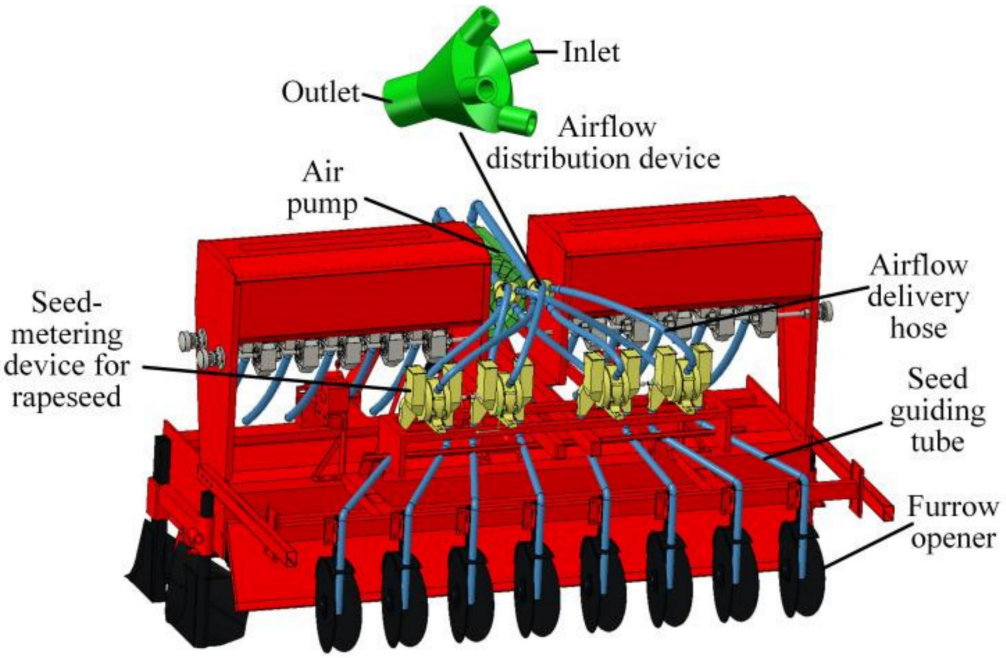

Figure 1. Structure of pneumatic system.

2.2. Working Principle of Airflow Distribution Device

The tractor's rear output shaft powers the air pump through the belt pulley when the pneumatic system is activated. Through the airflow delivery hose, which is linked to the pressure output of the air pump, the high-pressure airflow created by the air pump is transmitted to the two airflow distribution devices at positive and negative pressure. The pipe connects four inlets of a negative pressure airflow distribution device to four seed-metering devices. This article focuses solely on negative pressure air distribution systems since they primarily impact on the performance of rapeseed seed-metering equipment. The pneumatic system will cause pressure loss throughout the pipeline and local pressure loss during this procedure. However, it is difficult to decrease pressure loss throughout the pipeline by optimizing its structure since the distance between the air pump, airflow distribution device, and seed-metering device cannot be altered, and the pipeline arrangement is complex. The structural kinds and specifications of airflow distribution devices have a larger influence on the local pressure loss of pneumatic systems, and this may be exploited as a breakthrough in the optimization of pneumatic systems [14,15].

2.3. Structure of Airflow Distribution Device Parameters

2.3.1. Structural Design of Airflow Distribution Device

A pneumatic seed-metering equipment relies on an airflow distribution device to accomplish a succession of seeding activities, including seed filling, carrying, and falling [16]. Its fundamental structural structure is seen in Figure 2.

2.3.2. Design of Basic Structural Parameters of Airflow Distribution Device

Most pneumatic rapeseed seeders on the market produce negative pressure using an air pump [17]. The diameter of the air pump's exit is 48 mm, while the diameter of the seed-metering device's airflow input is 26 mm. To ensure the tightness of the pneumatic system and to account for the hose connection between the air pump, the seed-metering device, and the airflow distribution device, the outlet diameter of the air distribution device must match the diameter of the air pump's negative pressure outlet, and the inlet diameter must match the diameter of the seed-metering device's inlet.

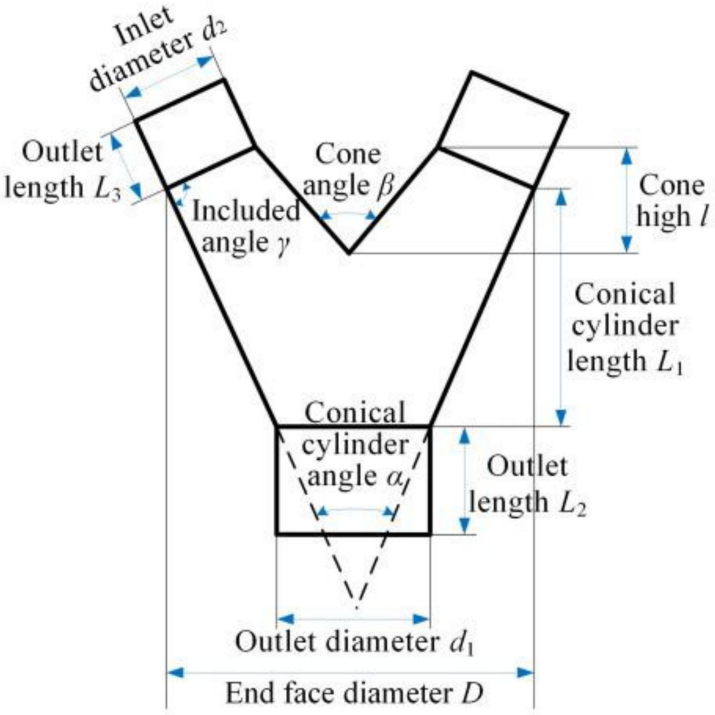

Figure 2. Structural parameters of an airflow distribution device.

The minimum diameter of the lower conical cylinder end face may be established using the outlet diameter of the airflow distribution device in conjunction with the number of outlets involved, as well as the thickness and installation gap of the hose. Currently, the end face is almost parallel to the end face of the outlet of the airflow distribution device. Figure 3 depicts the schematic diagram of the minimum end face diameter. We are able to discover a geometric relationship. The connection may be described as follows:

$$\begin{cases} Dm = \sqrt{2}\delta + \left(\sqrt{2}+1\right)d_2 \\ \delta = 2\delta_1 + \delta_2 \end{cases} \quad (1)$$

where, take δ_1 = 6 mm, δ_2 = 15 mm, and the minimum end face diameter $D_m \approx 101$ mm calculated by Formula (1).

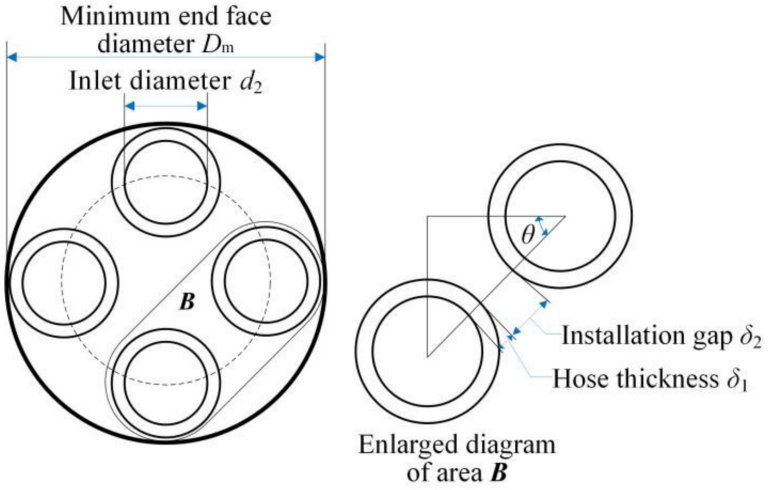

Figure 3. Schematic diagram of the minimum end face diameter.

Basic structural specifications are set in terms of installation and attachment of the hose, as well as the tightness, and overall size of the airflow distribution device in mind. The outlet diameter d_1 measures at 48 mm, the outlet length L_2 measures at 40 mm, the inlet diameter d_2 measures at 26 mm, the inlet length L_3 measures at 30 mm, the lower conical cylinder length L_1 measures at 60 mm, and the end face diameter D measures 110 mm.

2.3.3. Design of Key Structural Parameters of Airflow Distribution Device

We can derive some geometric relationships from Figure 3. The relationship can be expressed as follows:

$$\begin{cases} \tan\frac{\alpha}{2} = \frac{D-d_1}{2L_1} \\ 90^\circ - \frac{\alpha}{2} \le \gamma \le 90^\circ + \frac{\alpha}{2} \end{cases} \quad (2)$$

From Formula (2), when the length of lower conical cylinder L_1 is constant, the size of α is related to the end face diameter D, and the angle γ is related to the angle α. Putting the end face diameter D = 110 mm into Formula (2) can be obtain that α = 54.6°, and the value range of γ is 62.7° $\le \gamma \le$ 117.3°.

$$\tan = \frac{\beta}{2} = \frac{2L_1 \tan\frac{\alpha}{2} + d_1 - 2d_2 \sin\left(\gamma + \frac{\alpha}{2}\right)}{2l} \quad (3)$$

where, the height range of the cone is $0 \le l \le L_1 + L_2 = 100$ mm. According to Formula (3), the size of angle β is related to angle γ and height l. When γ = 62.7°, substitute into Formula (3), we can derive the range of angle β is 32.3°$\le \beta \le$180°; when γ = 117.3°, we can derive the range of angle β is 57.6° $\le \beta \le$ 180°. We may determine that the range of angle β shrinks as angle γ increases. In order to study the influence of angle β on the negative pressure loss of airflow distribution device when angle γ takes different values, angle β should take the same value. Meanwhile, it satisfies the value conditions of angle β when angle γ is different, so the range of angle β is 57.6° $\le \beta \le$ 180° when the simulation structure is optimized.

3. Materials and Methods

In this paper, three types of airflow distribution devices were compared using Fluent software, and the ideal structural type was chosen. Additionally, optimum orthogonal testing of structural parameters was conducted.

3.1. Model Building

Utilizing Solidworks, create three distinct structural types of airflow distribution devices as 3D models (Figure 4). The variation in structure consists of the form of the airflow-guiding chamber and the placement of four inlets. The first kind employs a cylindrical airflow-directing chamber and circular outlet distribution; the second type utilizes a conical cylinder airflow-guiding chamber and circular outlet distribution; the third type utilizes a conical cylinder airflow-guiding chamber and conical outlet distribution. Import the 3D model into the workbench program, choose the internal fluid region of the flow distribution device using the "filling" tool, and mesh the internal fluid area using the "mesh" tool. The tetrahedral mesh was employed, the maximum number of boundary layers on the model wall was 5, the growth rate was set to 1.2, and the transition ratio was left at its default value of 0.272 [18].

In the presimulation, four gradients of maximum surface size were set to 1 mm, 2 mm, 4 mm, and 8 mm, and the inlet negative pressure for the simulation was set at 2000 pa. The results indicated that the maximum surface size was set to 1 mm and 2 mm, and the simulation results were comparable. This indicated that the susceptibility of the calculation results to grid density changes was minimized and the grid independence requirements were met. While the maximum surface dimensions are set to 4 mm and 8 mm, the relative inaccuracy is significant. Considering the simulation accuracy and simulation time requirements, the maximum surface size is set at 2 mm.

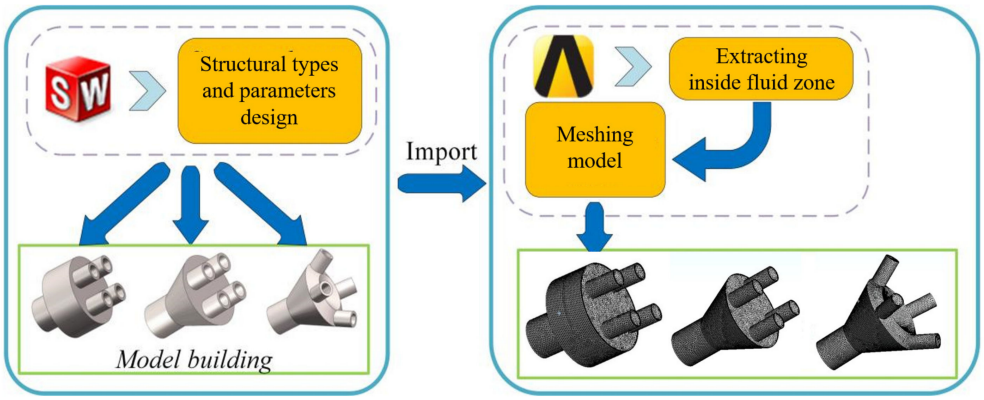

Figure 4. Model building and meshing.

3.2. Simulation Settings and Evaluation Indicators

3.2.1. Simulation Settings

For field work, the pneumatic metering equipment created by the research team has a negative pressure of 1000 to 2500 Pa [19], and the Reynolds number $Re = 4.9 \times 105 > 4000$ can be obtained according to the literature [18], so the research object of this study should choose the incompressible turbulence model. In actual work, the outlet negative pressure is provided by an air pump, and so the outlet negative pressure is generally fixed. In the boundary condition setting, the pressure-outlet and pressure-inlet were applied at the outlet and inlet of the airflow distribution device, respectively [20].

3.2.2. Evaluation Indicators of Simulation

According to the published research [21,22], the force of airflow on the rapeseed is proportional to the airflow pressure during the process of seed-plate hole adsorption. When the pressure at the airflow outlet is constant, the greater the airflow inlet pressure is, the lower the negative pressure loss rate will be too. Consequently, the negative pressure loss and negative pressure loss rate between the inlet and exit may be used to evaluate the operation of an airflow distribution device. It is described as follows:

$$\begin{cases} \Delta P = |P_i - P_o| \\ R_s = \frac{\Delta P}{P_i} \times 100\% \end{cases} \quad (4)$$

where, ΔP is the absolute value of pressure loss of the outlet and the inlet, Pa; R_s is the negative pressure loss rate, %; P_i is the average value of negative pressure of four inlets, Pa; P_o is the average value of negative pressure of the outlet, Pa.

3.3. Simulation Method

3.3.1. Selection of Structural Type

In order to determine the causes of negative pressure loss and to comprehend the properties of the internal airflow field of three structural kinds, the negative pressure was utilized as a test factor. During the simulation test of three types of airflow distribution devices, the negative pressure loss and negative pressure loss rate were utilized as evaluative indications. Set the outlet negative pressure values to 500, 1000, and 1500 Pa, import three structural type models that were meshed in preprocessing into Fluent, choose the k-model as the turbulence model, and set the continuity equation's convergence condition to $1e^{-4}$. Simultaneously, four monitoring windows were established to monitor the pressure change of the airflow distribution device's four inlets. The semi-implicit method (Simple) of the pressure coupling equation group was chosen for solving purposes, and the pressure equation's order of solution was set to second [23].

3.3.2. Optimization of Structural Parameters

In order to explore the influence of key structural parameters on the performance of the optimal airflow distribution device, we took the angles β and γ as test factors. The negative pressure loss and negative pressure loss rate were indicators. The value range of angle β was $57.6^\circ \leq \beta \leq 180^\circ$, and the range of angle γ was $62.7^\circ \leq \gamma \leq 117.3^\circ$. Table 1 demonstrates the levels of each factor. Changes were made to the optimum model's structural parameters based on the design of the orthogonal experiment, and Workbench software was used to mesh the model. The data are then transferred into the simulation program Fluent. According to the simulation results presented in the previous section, the negative pressure loss rate remained almost identical when structural types and characteristics were held constant, and only the outlet negative pressure was altered. Therefore, the outlet negative pressure of the airflow distribution device was fixed at 1000 Pa, with the same boundary conditions and simulation environment as described previously.

Table 1. Experiment factors code.

Code	Factors	
	Angle β/(°)	**Angle γ/(°)**
−1.414	57.6	62.7
−1	75.5	70.7
0	118.8	90
1	162.1	109.3
1.414	180	117.3

3.4. Bench Test

3.4.1. Materials and Equipment of Bench

The test was conducted on the bench of a pneumatic rapeseed sowing system. Figure 5 depicts its primary construction and air pressure monitoring system. The primary components of the test bench were an air pump, a stepper motor, an airflow distribution device, a transition shaft, and a pneumatic rapeseed seed-metering device. The primary components of the air pressure monitoring system are a pressure sensor, an upper computer, a data collection card, and a direct-current supply. The test material chose the "Sheng you 664" seeds for rapeseed. Seeds have a moisture content of 3.54% and a weight per thousand grains of 4.66 kg.

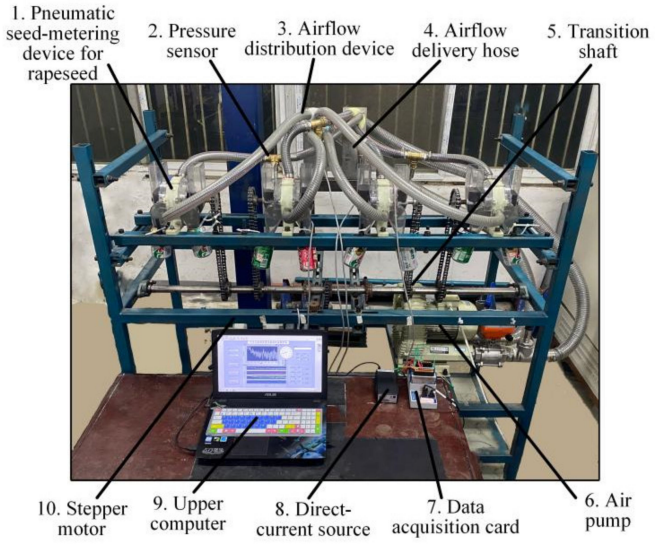

Figure 5. Main structure of pneumatic rapeseed seeding device and air pressure monitoring system. Note: The position 1 shows the installation position of air distribution device. During the test, the different structure types of air distribution device can be replaced for testing.

3.4.2. Test Method of Bench

According to the ideal structural characteristics of the simulation model acquired during orthogonal testing, three types of airflow distribution devices were manufactured using 3D printing technology and installed at position 2 in Figure 6. We took the structural type of the model, working negative pressure and seed plate rotational speed as test factors, and negative pressure loss rates and variation coefficients of seeding quantity in each row as indicators. On a test bench, a full factor test was conducted to determine the effectiveness of the airflow distribution device and its effect on the seed-metering device. In hilly and small-field areas, the maximum operating speed of a pneumatic seeder for rapeseed was typically 7 km/h [24]. Selecting Dongfanghong-LY954 as the traction power, we chose three standard tractor gears: slow I gear, slow III gear, and slow IV gear. The relative operating speeds were 2.17, 4.15, and 6.68 km/h. The theoretical planting distance for rapeseed was fixed at 50 mm. According to the conversion formula between tractor operating speed and seed plate rotating speed [25], the seed plate rotational speeds were determined to be 20.09, 38.43, and 61.85 r/min, respectively. The working negative pressure was determined using the same gradients as in the simulation test, namely 500, 1000, and 1500 Pa. In the experiment, there were 27 groups, and the levels of each variable are indicated in Table 2.

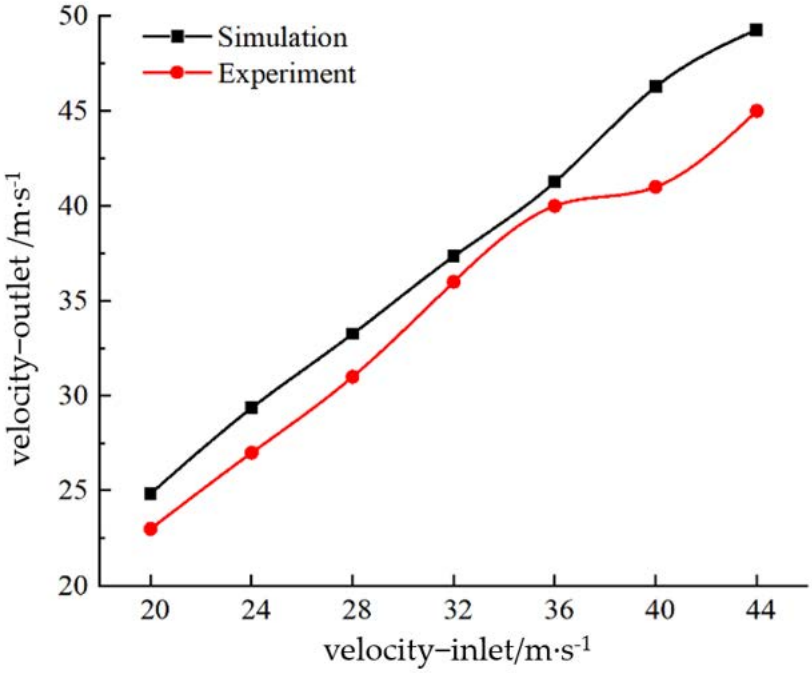

Figure 6. Comparison between experimental and simulation results.

Table 2. Test factor levels.

Levels	Factors		
	Structural Types *A*	**Seed Plate Rotational Speed *B*/(r·min^{-1})**	**Working Negative Pressure *C*/Pa**
1	Cylindrical circular-arranged	20.09	500
2	Conical cylinder circular-arranged	38.43	1000
3	Conical cylinder conical-arranged	61.85	1500

During the test, we activated the control box's power to normalize the air pump function, read the negative pressure at the outlet of the airflow distribution device using the

air pressure monitoring system that was designed based on previous research, and adjusted the working negative pressure to the required level. We measured the negative pressure of the seed-metering device's outflow and input within three minutes of normal operation and used the average as the negative pressure under these conditions. After three minutes of seeding, the quality of the seeds expelled from each seed-guiding tube was determined using an electronic balance. Each set of tests was done three times, and after each type of test, the airflow distribution equipment was changed. Then, we calculated the negative pressure loss rate and variation coefficient of seeding quantity in each row according to the formula below and the GB/T9478-2005 grain test method [26]. The calculation formula is as follows:

$$\begin{cases} Rs = \frac{|P_i - P_o|}{P_i} \times 100\% \\ m = \frac{\sum_{i=1}^{N} X_i}{N} \\ CV = \frac{\sqrt{\frac{1}{N-1}\sum_{i=1}^{n}(X_i - m)^2}}{m} \end{cases} \quad (5)$$

where, R_s is the negative pressure loss rate, %; P_i is the average value of the inlet, kPa; P_o is the average value of the outlet, kPa; m is the average value of the total quality of rapeseed, g; CV is the variation coefficient of seeding quantity in each row, %; N is the number of seed guiding tubes (N = 8); X_i is the quality of rapeseed discharged from the i-th seed guiding tube, g.

4. Results and Discussion

4.1. Model Validation

The negative pressure real-time monitoring system built by the study team was utilized to monitor the valve mechanism in real time, and the results of airflow inlet and outflow velocities were measured as depicted in Figure 6. Overall, the outlet velocity increases with the inlet velocity in both models and experiments, however the predicted velocity is slightly higher than the experimental results by 8%.

4.2. Analysis of Simulation Results

4.2.1. Analysis of Structural Type

Figure 7 depicts the pressure and velocity of the airflow field for three structure types under 1000 Pa of negative pressure. According to the first two types of pressure diagrams, there is a large pressure drop in the airflow-guiding chamber at the airflow exit and in the airflow-guiding chamber's conical cylinder wall. Negative pressure airflow created by the air pump entered the airflow distribution device and impacted with the inner wall of the airflow-guiding chamber, causing relative motion between the airflow and the distribution device. The velocity diagram reveals that the relative motion of the objects produced the change in airflow direction. The other portion of the airflow created turbulence in the middle of the airflow-directing chamber, as well as the conversion of kinetic energy into internal energy and its consumption, which showed itself in two ways: negative pressure loss and speed loss. According to the third structural kind of pressure diagram, there is a large decrease in pressure near the top of the airflow-directing chamber, where the airflow converges. This occurred owing to the airflows' collision at the top of the airflow-directing chamber, which resulted in negative pressure and velocity loss. When the outlet negative pressure remains constant, the input negative pressure of the third structural type is the greatest. We concluded that the type with conical inlets not only reduced the likelihood of airflow collision with the inner wall of the airflow distribution device, but also that the interaction between the airflow and the inner wall is greater than that between the airflows. Therefore, the conical cylinder conical-arranged airflow distribution device has less negative pressure loss and velocity loss than the previous two types.

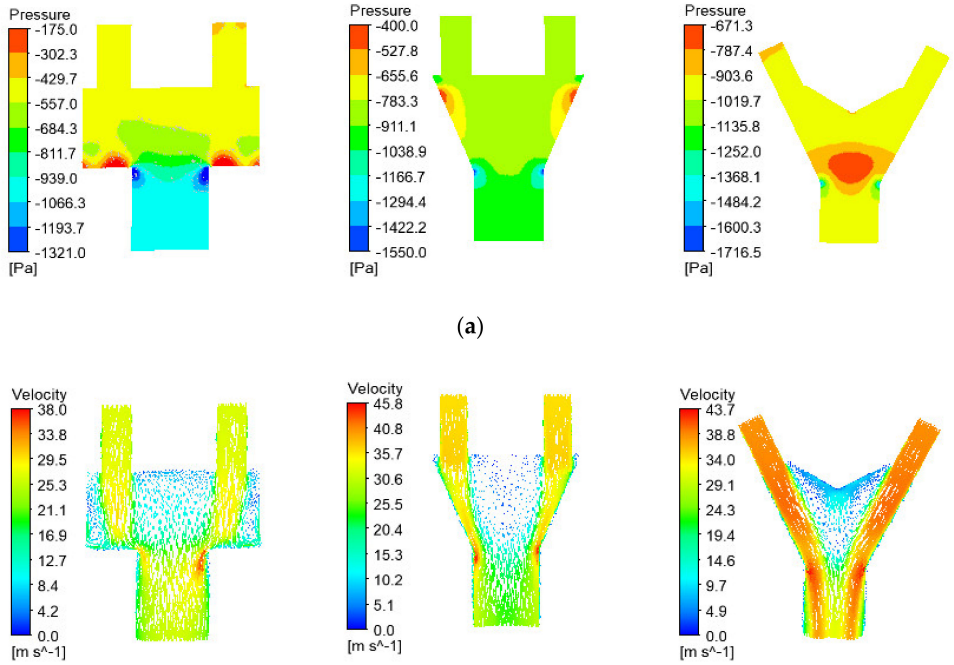

Figure 7. Pressure and velocity of airflow field of three structural types. (**a**) Pressure of airflow field. (**b**) Velocity of airflow field.

Table 3 displays the simulation outcomes for several structure kinds. Under the same negative outlet pressure, the first kind had the highest negative pressure loss rate, while the third type exhibited the lowest. However, when using the same model with various outlet negative pressure settings, each model's negative pressure loss rate was essentially the same and did not vary considerably as the negative pressure increased. We extrapolated that the variation in structural type caused the airflow to touch and collide in a different manner, resulting in a significant variance in negative pressure loss. When the structural kinds and specifications were fixed, and the setting for the negative pressure at the outlet was altered, the meeting and collision of airflows did not change. As a result, there was little change in the loss rate since the negative pressure at the intake rose by the same amount. In the real bench test, the impact of the complete structure of the pneumatic system and the airflow delivery hose attached to it must be taken into account so that it will be changed with the change of negative pressure.

Table 3. Simulation results of three structural types.

Types	Outlet Negative Pressure/Pa	Inlet Negative Pressure/Pa	Negative Pressure Loss/Pa	Negative Pressure Loss Rate/%
Cylindrical circular-arranged	500	231.27	268.73	53.75
	1000	468.01	531.99	53.20
	1500	715.81	784.19	52.28
Conical cylinder circular-arranged	500	375.74	124.26	24.85
	1000	748.52	251.48	25.15
	1500	131.76	368.24	24.55
Conical cylinder conical-arranged	500	434.51	65.49	13.10
	1000	876.75	123.25	12.33
	1500	1319.55	180.45	12.03

Note: The inlet negative pressure was the average value of four inlet negative pressures of the airflow distribution device.

4.2.2. Analysis of Parameter Optimization Results

From the above simulation study, it is possible to determine that negative pressure loss was the result of a collision between the airflow and the inner wall. This type of contact resulted in turbulence and decreased airflow velocity. Figures 8 and 9 depict the pressure and velocity of the optimal structural type with different structural parameters during the orthogonal test. Figure 8 demonstrates that the angle mostly impacted the direction of airflow entering four inlets. When $\gamma < 90^{\circ}$, it was easy for airflow to contact and collide with the inner wall in the middle of airflow-guiding chamber and lots of turbulence was produced, which caused numerous pressure and velocity loss; when $\gamma > 90^{\circ}$, it was not easy to collide with the inner wall, but the time of contact collision between the airflows was advanced, which prolonged the interaction time between the airflows, and most of airflow was consumed by energy conversion.

Angle β mostly impacted the size of the turbulence region generated. When β was small, the interior space of the airflow-directing chamber was also modest. Even though the airflow collision occurred, turbulence formation within the airflow-directing chamber proved difficult. However, it enhanced the contact intensity between the airflows, and the vast majority of the airflow's kinetic energy was transformed into internal energy for consumption. In contrast, when β was large, the majority of the airflow generated turbulence in the chamber's centre, and a minor quantity of airflow caused energy conversion between the airflow interactions. Consequently, it was necessary to optimize the structural parameters of the optimal type in order to reduce the possibility of contact collision between the airflow and the inner wall, thereby effectively reducing the negative pressure loss rate and enhancing the performance of the airflow distribution device.

The results of the orthogonal simulation test are displayed in Table 4. In order to determine the relevance of angles β, γ and negative pressure loss rate, variance analysis was performed on simulation data using Design-Expert software, and the findings are presented in Table 5.

Table 4. Orthogonal test results.

NO	Angle β/(°)	Angle γ/(°)	Negative Pressure Loss Y_1/Pa	Negative Pressure Loss Rate Y_2/%
1	180	90	165.48	16.55
2	118.8	90	125.65	12.57
3	118.8	62.7	436.24	43.62
4	75.5	70.7	317.02	31.70
5	162.1	109.3	257.05	25.71
6	75.5	109.3	206.15	20.62
7	118.8	90	115.74	11.57
8	162.1	70.7	300.34	30.03
9	57.6	90	132.39	13.24
10	118.8	90	121.39	12.14
11	118.8	90	113.99	11.40
12	118.8	90	120.09	12.01
13	118.8	117.3	294.58	29.46

It can be seen from Table 4 that angle β has a significant effect on the negative pressure loss rate, and angle γ has a very significant effect on the negative pressure loss rate. The interaction between angle β and γ also has a significant impact on the negative pressure loss rate, so it can be optimized as a key parameter of an airflow distribution device.

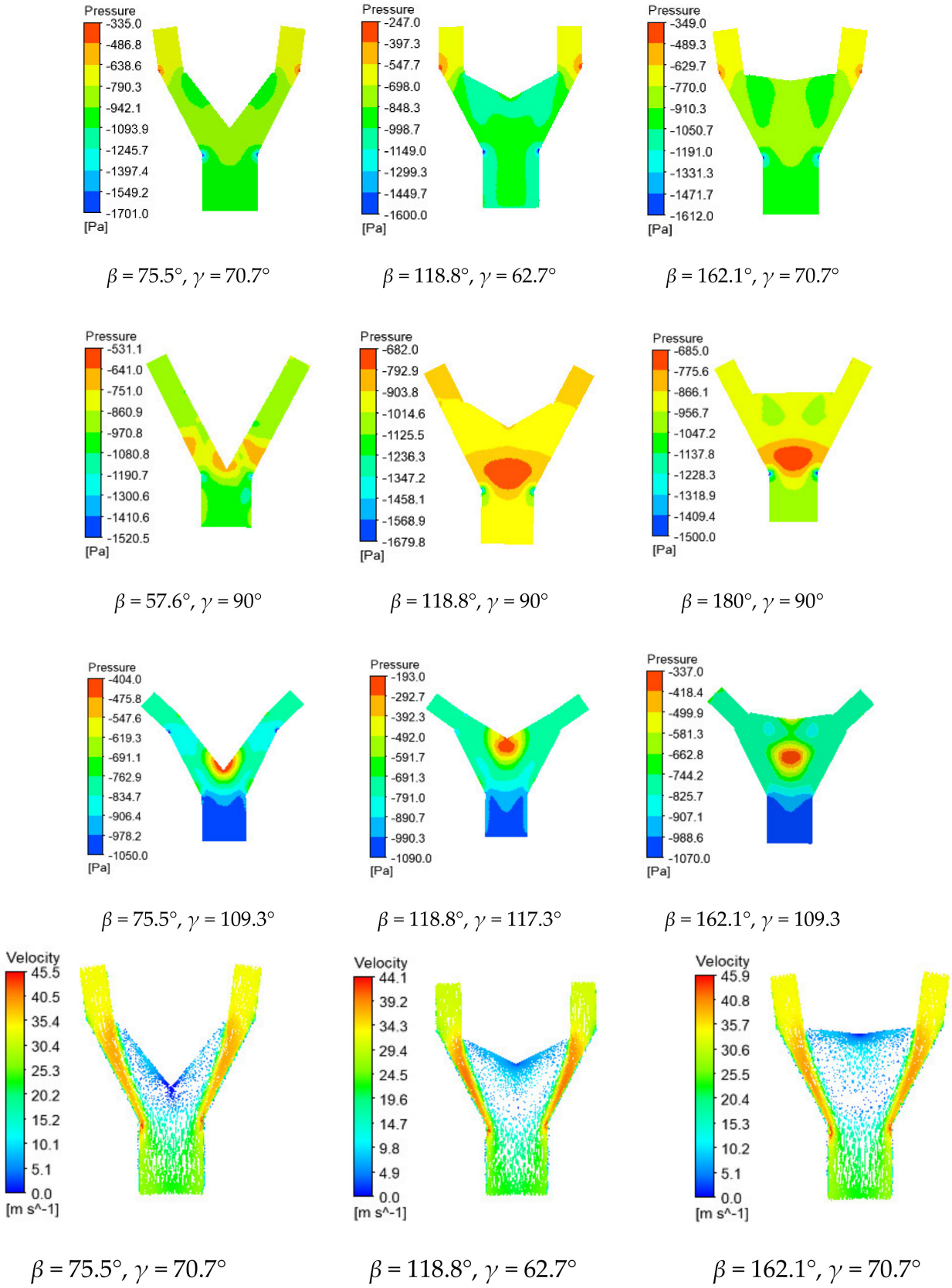

Figure 8. The pressure airflow field of optimal structural type with different structural parameters.

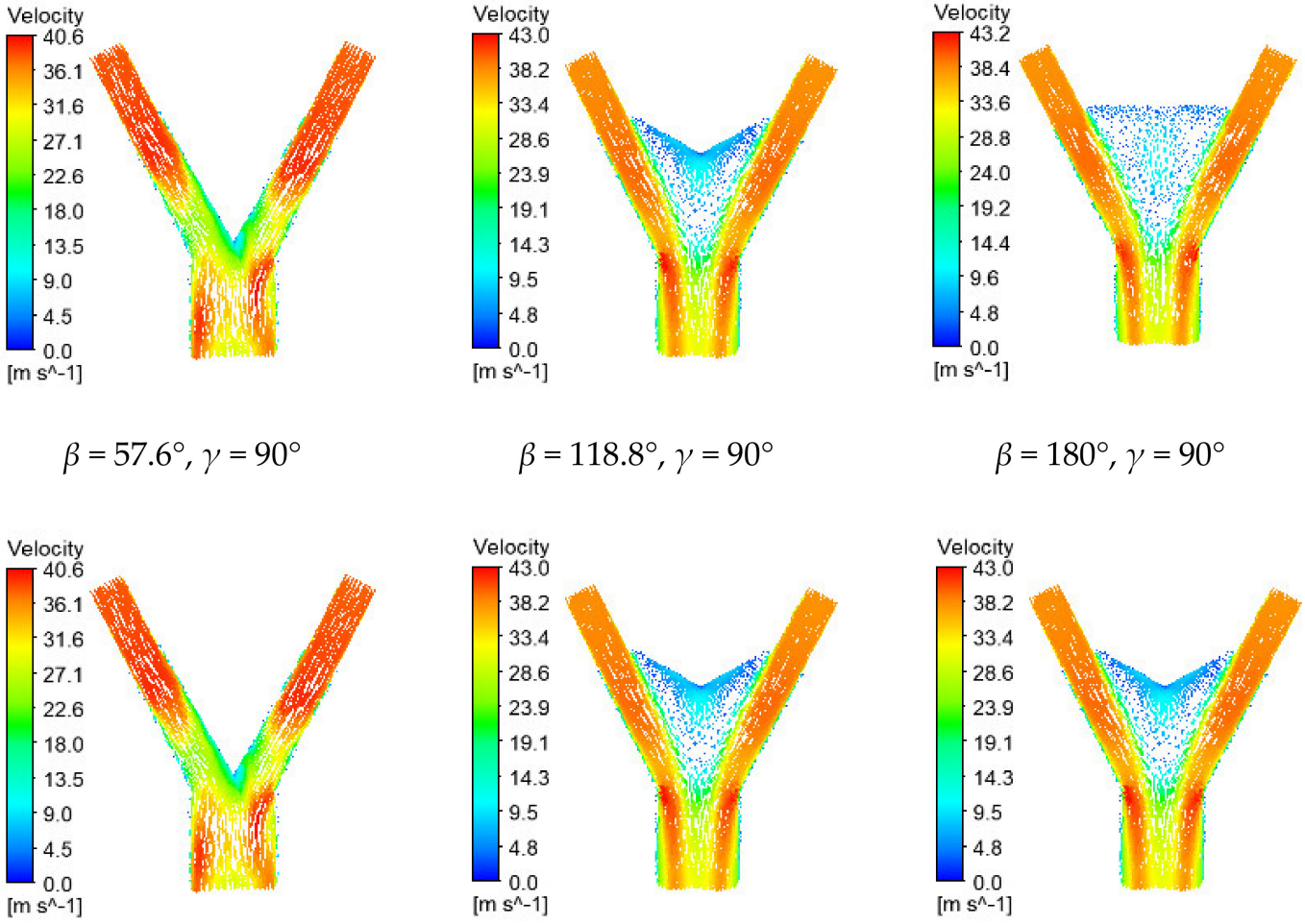

Figure 9. The velocity airflow field of optimal structural type with different structural parameters.

Table 5. Variance analysis.

Sources	Square Sum	Degree of Freedom	Mean Square	*F* Value	*p* Value
β	8.20	1	8.20	8.02	0.0253 *
γ	156.87	1	156.87	153.32	<0.0001 **
$\beta\gamma$	11.42	1	11.42	11.17	0.0124 *
γ^2	23.52	1	23.52	22.99	0.0020 **
β^2	1115.20	1	1115.20	1089.97	<0.0001 **
Residual	7.16	7	1.02		
Total	1299.11	12			

Note: * indicates significant ($0.01 < p < 0.05$), ** is highly significant ($p < 0.01$).

The lower the negative pressure loss, the lower the negative pressure loss rate, and the better distribution performance. According to the results in Table 4, we took the negative pressure loss rate as the target of optimization, and used Design-Expert software to optimize the parameters of the model in order to obtain the best optimization results. By optimization, the best parameter combination was obtained that $\beta = 103.0°$, $\gamma = 91.9°$, where the negative pressure loss rate was the lowest. At this time, the negative pressure loss was 113.7 Pa, and the negative pressure loss rate was 11.37%.

4.3. Results and Analysis of Bench Test

A significant analysis was performed on the seed plate rotating speed and working negative pressure for the three distinct kinds was determined (Figure 10). It is evident that the structural type, seed plate rotating speed, and working negative pressure all influence the negative pressure loss rate and variation coefficient of seeding quantity in each row. The negative pressure loss rate and variation coefficient of seeding quantity in each row rise dramatically as the rotational speed of the seed plate increases. When the rotating speed of the seed plate was 20.09 r/min, the negative pressure loss rate and variation coefficient of seeding quantity in each row were the lowest. When the rotating speed of the seed plate was 61.85 r/min, the negative pressure loss rate and variation coefficient of seeding quantity in each row were inversely proportional. With an increase in operating negative pressure, the negative pressure loss rate and variance coefficient of seeding quantity per row decreased dramatically. The negative pressure loss rate and variation coefficient of seeding quantity in each row were greatest when the working negative pressure was 500 Pa. When the pressure was 1500 Pa, the negative pressure loss rate and seeding amount variation coefficient in each row were opposite to each other in values.

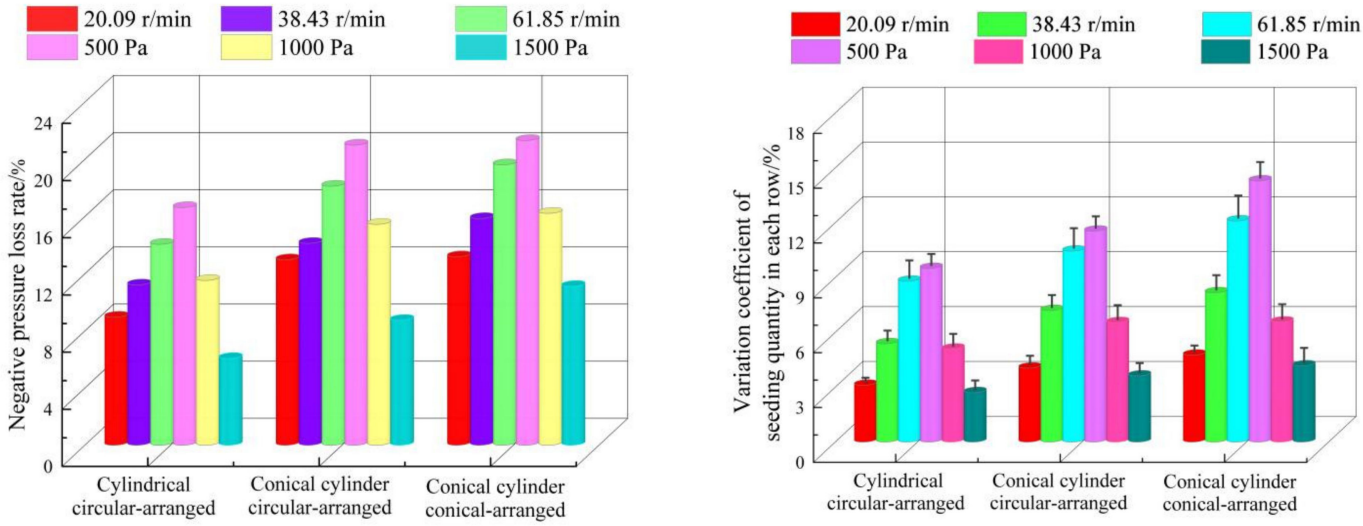

Figure 10. The significance analysis of three structural types.

This may be due to a reduced likelihood of internal airflow collisions, which thereby reduces turbulence and makes it simpler for air to travel through the apparatus. Consequently, the device has superior distribution performance even at lower negative pressure. As the seeder seeded at a slower rate in the field, the negative pressure decreased significantly. Comparing the type of conical cylinder conical-arranged air distribution device to the type of cylindrical circular-arranged device would reduce the negative pressure loss rate and variation coefficient of seeding quantity in each row by 6.25 and 3.48%, respectively, when the negative pressure dropped to 500 Pa.

The variance analysis is displayed in Table 6. The negative pressure loss rate and the fluctuation coefficient of the number of seeds in each row are significantly influenced by the three single factors. When two of the three components are present, they have little impact on the negative pressure loss rate. Working negative pressure interacts with the other two parameters, and this interaction has a significant impact on the coefficient of variance for the quantity of seeds in each row. The literature [18] indicated that the uniformity of the number of seeds sown in each row is the most critical aspect affecting the performance of a seed-metering system and the growth of rapeseed. When there was low negative pressure or a quick reduction in negative pressure, the appropriate design of the airflow distribution device helps to limit the loss of negative pressure during the seeding process. Additionally, it produced more uniform plant spacing in each row.

Table 6. Variance analysis.

Sources of Variation	Negative Pressure Loss Rate R_s					Variation Coefficient of Seeding Quantity in Each Row *CV*				
	Square Sum	Degree of Freedom	Mean Square	*F* Value	*p* Value	Square Sum	Degree of Freedom	Mean Square	*F* Value	*p* Value
A	113.473	2	56.736	29.54	<0.0001 **	35.596	2	17.798	58.20	<0.0001 **
B	142.537	2	71.268	37.11	<0.0001 **	198.135	2	99.067	323.98	<0.0001 **
C	545.322	2	272.661	141.96	<0.0001 **	324.289	2	162.4	530.26	<0.0001 **
AB	3.179	4	0.795	0.41	0.795	3.574	4	0.894	2.92	0.092
AC	3.955	4	0.989	0.51	0.728	9.545	4	2.386	7.80	0.007 **
BC	24.002	4	6.001	3.12	0.080	40.057	4	10.014	32.75	<0.0001 **
Residual	15.366	8	1.921			2.446	8	0.306		
Total	847.834					613.641				

Note: ** is highly significant ($p < 0.01$).

The Origin software was used to correlate the test results for the correlation test in order to explore the correlation between the negative pressure loss rate of the airflow distribution device and the variation coefficient of seeding quantity in each row of the seed-metering device under the interaction of seed plate rotational speed and working negative pressure. The correlation coefficient used was Pearson, and the findings are presented in Table 7.

Table 7. Correlation test.

Indexs	Negative Pressure Loss Rate	Variation Coefficient of Seeding Quantity in Each Row
Mean	13.087	4.168
Standard deviation	5.025	3.001
Total	209.39	66.69
Pearson correlation	0.74502 *	
p value	$9.275e^{-4}$	

Note: * indicates that the correlation is significant at the 0.05 level.

Under the interaction impact of seed plate rotating speed and working negative pressure, Table 7 indicates that the negative pressure loss rate has a substantial positive association with the variation coefficient of seeding quantity in each row. As the rate of negative pressure loss dropped, the coefficient of variance of seeding quantity in each row of seed-metering devices also fell. Therefore, we may boost the seed-metering performance of seed-metering devices by upgrading the kind of airflow distribution device and optimizing the structural characteristics to satisfy the rapeseed agronomical seeding requirements.

4.4. Field Test

From 8 November to 12 November 2021, a field test of rapeseed planting was conducted in Huaining, Anhui Province, in order to further confirm the distribution performance of the airflow distribution device in the field. Prior to seeding, rice was the crop being cultivated, and the height of the stubble was 0.25~0.40 m. Use the following steps to replicate this method. Select a Dongfanghong-LY954 wheeled tractor and a 2BFQ-8 pneumatic rapeseed seeder from Hualei Agricultural Machinery Company. Use slow II gear for sowing during the sowing procedure. We used a negative pressure monitoring system to collect actual working negative pressure during the test, replaced various structural types of airflow distribution devices for the test, and chose the negative pressure in the range of 1000–2500 Pa to calculate the negative pressure loss rate of each structural type. Specific field experiments are shown in Figure 11.

The weighting approach was used to determine the variation coefficient of the seeding amount in each row after each group of experiments had been completed. Uneven ground and some vibration from the engine during operating in the field had an impact on the rapeseed seeder. The bench test and field test both included several mistakes. The findings of the field tests are depicted in Figure 12.

Figure 11. Field test.

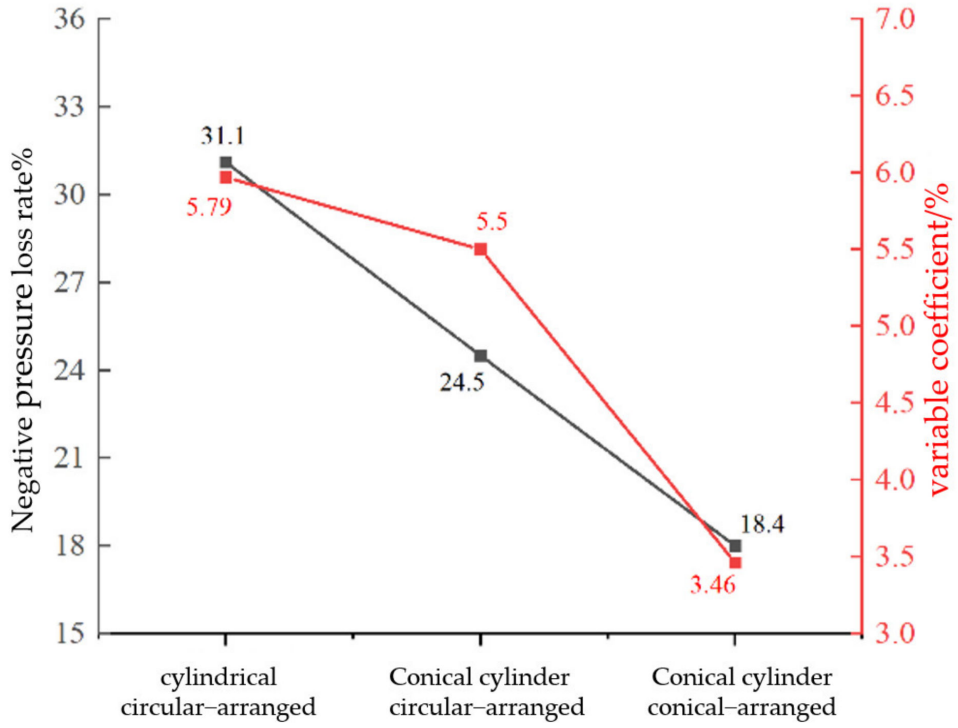

Figure 12. Negative pressure loss rate and variation coefficient.

The conical cylinder conical-arranged device has a loss rate of negative pressure of 18.1%, whereas the other two models have loss rates of 24.5% and 31.0%, respectively. The coefficient of variation of sowing amount per row was 3.46%, 5.50%, and 5.97%, respectively. Field studies showed that creating and optimizing the structure and specifications of the airflow distribution device increased the seeding performance of seed-metering devices. Figure 13 depicts the rapeseed field trials and seeding.

Figure 13. Sowing for rapeseed.

5. Conclusions

We carried out an airflow field study of the air distribution device which influenced its airflow transmission in order to enhance the seeding performance of pneumatic seed-metering systems for rapeseed when negative pressure decreases significantly. A device was created for distributing airflow in a conical shape. The following were the conclusions:

(1) An airflow field analysis of an airflow distribution device was conducted using Fluent simulation. From the perspective of fluid kinematics, a cone-column conical-arranged type of airflow distribution device was designed and the reasons for negative pressure loss were analyzed. Through orthogonal tests, the structural parameters were optimized; when $\beta = 103.0^{\circ}$, $\gamma = 91.9^{\circ}$, the negative pressure loss rate of the airflow distribution device was the lowest.

(2) The results of the bench test showed that three elements had extremely substantial influence on both the variation coefficient of seeding quantity in each row and the negative pressure loss rate. There also existed a strong positive connection between the latter two mentioned factors. The variation coefficient of the quantity of seeding in each row of the seed-metering device and the negative pressure loss rate of the best structure type both decreased when the negative pressure fell to 500 Pa, by 6.25% and 3.48%, respectively.

(3) Field tests showed that the airflow distribution device's negative pressure loss rate was less than 20%, and that the seed-metering device's variation coefficient of seeding quantity in each row was less than 3.5%. These results can help the seed-metering device's seeding performance and help it to meet the agronomic requirements for planting rapeseed.

Author Contributions: Conceptualization, Z.L.; methodology, H.Z.; software, H.Z.; validation, Y.C.; formal analysis, R.X.; investigation, J.D.; resources, Z.L.; data curation, X.G.; writing—original draft preparation, H.Z.; writing—review and editing, H.Z.; supervision, Z.L.; project administration, Y.C.; funding acquisition, Z.L. All authors have read and agreed to the published version of the manuscript.

Funding: This study came from the National Natural Science Foundation of China: adsorption mechanism and mechanism of rapeseed high-speed precision sowing with grooved teeth directional disturbance (51805004).

Institutional Review Board Statement: Not applicable.

Informed Consent Statement: Not applicable.

Data Availability Statement: The data presented in this study are available on request from the corresponding author.

Acknowledgments: We thank the engineering training center of AnHui Agricultural University for providing the test site.

Conflicts of Interest: The authors declare no conflict of interest.

References

1. Wang, H.Z.; Yin, Y. Analysis and strategy for oil crop industry in China. *Chin. J. Oil Crop Sci.* **2014**, *36*, 414–421.
2. Liao, Q.X.; Lei, X.L.; Liao, Y.T.; Ding, Y.C.; Zhang, Q.S. Research progress of precision seeding for rapeseed. *Trans. Chin. Soc. Agric. Mach.* **2017**, *48*, 1–16.
3. Li, Z.Q.; Tang, C.Z.; Li, M.; Luo, H.F.; Wu, M.L. Parameter optimization and validation experiment on jet pipe of pneumatic pollination. *Trans. Chin. Soc. Agric. Mach.* **2015**, *31*, 68–75.
4. Liao, Q.X.; Li, J.B.; Tan, G.L. Analysis on air current field of pneumatic precision metering device for rapeseed. *Trans. Chin. Soc. Agric. Mach.* **2009**, *40*, 78–82.
5. Li, Z.H.; Wang, D.C.; Liu, G.L.; Yang, M.S.; Wang, Z.H. CFD simulation and improvement of air-stream distributive metering device. *Trans. Chin. Soc. Agric. Mach.* **2009**, *40*, 64–68.
6. Lei, X.L.; Liao, Y.T.; Zhang, Q.S.; Wang, L.; Liao, Q.X. Numerical simulation of seed motion characteristics of distribution head for rapeseed and wheat. *Comput. Electron. Agric.* **2018**, *150*, 98–109. [CrossRef]
7. Lei, X.L.; Hu, H.J.; Yang, W.H.; Liu, L.Y.; Liao, Q.X.; Ren, W.J. Seeding performance of air-assisted centralized seed-metering device for rapeseed. *Int. J. Agric. Biol. Eng.* **2021**, *14*, 79–87. [CrossRef]
8. Ahmad, F.; Adeel, M.; Qiu, B.J.; Ma, J.; Shoaib, M.; Shakoor, A.; Chandio, F.A. Sowing uniformity of bed-type pneumatic maize planter at various seedbed preparation levels and machine travel speeds. *Int. J. Agric. Biol. Eng.* **2021**, *14*, 165–171. [CrossRef]
9. Liu, J.X.; Wang, Q.J.; Li, H.W.; He, J.; Lu, C.Y. Numerical analysis and experiment on pneumatic loss characteristic of pinhole-tube wheat uniform seeding mechanism. *Trans. Chin. Soc. Agric. Mach.* **2020**, *51*, 29–37.
10. Yatskul, A.; Lemiere, J.P. Establishing the conveying parameters required for the air-seeders. *Biosyst. Eng.* **2018**, *166*, 1–12. [CrossRef]
11. Yatskul, A.; Lemiere, J.P.; Cointault, F. Influence of the divider head functioning conditions and geometry on the seed's distribution accuracy of the air-seeder. *Biosyst. Eng.* **2017**, *161*, 120–134. [CrossRef]
12. Yin, X.W.; Yang, L.; Zhang, D.X.; Cui, T.; Han, D.D.; Zhang, T.L.; Yu, Y.M. Design and experiment of balance and low-loss air allotter in air pressure maize precision planter. *Trans. Chin. Soc. Agric. Mach.* **2016**, *32*, 9–17.
13. He, S. *Analysis and Experiment on the Adsorption Mechanism of the Perturbation Pneumatic Precision Peed Metering Device for Rapeseed*; Anhui Agricultural University: Hefei, China, 2021.
14. Wang, Y.W.; Tang, C.; Wang, J.; Hu, J.B.; Ren, Q.F. Optimization and experiment on pollination tube of collision and air-blowing hybrid rice pollination machine. *Trans. Chin. Soc. Agric. Mach.* **2015**, *31*, 101–106.
15. Lei, X.L.; Liao, Y.T.; Wang, L.; Wang, D.; Yao, L.; Liao, Q.X. Simulation of gas-solid two-phase flow and parameter optimization of pressurized tube of air-assisted centralized metering device for rapeseed and wheat. *Trans. Chin. Soc. Agric. Mach.* **2017**, *33*, 67–75.
16. Li, Z.D.; Li, S.S.; Cao, X.Y.; Lei, X.L.; Liao, Y.T.; Wei, Y.P.; Liao, Q.X. Seeding performance experiment of pneumatic-typed precision centralized metering device. *Trans. Chin. Soc. Agric. Mach.* **2015**, *31*, 17–25.
17. Wang, L.; Liao, Q.X.; Liao, Y.T.; Gao, L.P.; Xiao, W.L.; Chen, H. Effects of distributor types on fertilizing performance in an air-assisted applicator. *Trans. Chin. Soc. Agric. Mach.* **2021**, *37*, 24–34.
18. Dai, Y.Z.; Luo, X.W.; Wang, Z.M.; Zeng, S.; Zang, Y.; Yang, W.W.; Zhang, M.; Wang, B.; Xing, H. Design and experiment of rice pneumatic centralized seed distributor. *Trans. Chin. Soc. Agric. Mach.* **2016**, *32*, 36–42.
19. Li, Z.D.; Yang, W.C.; Wu, Y.Y.; He, S.; Wang, W.W.; Chen, L.Q. Performance analysis and experiments of seed filling assisted by groove-tooth of pneumatic disc precision metering device for rapeseed. *Trans. Chin. Soc. Agric. Mach.* **2020**, *36*, 57–66.
20. Zhang, M.; Wu, C.Y.; Zhang, W.Y. Airflow field simulation on suction nozzle of cupule-type disseminator for rice seedling. *Trans. Chin. Soc. Agric. Mach.* **2011**, *27*, 162–167.
21. Xu, K.; Ge, Y.Y.; Xiao, M.H.; Kang, M.; Ni, J. Design of a straw picking and cutting device. *Int. J. Agric. Biol. Eng.* **2021**, *14*, 93–98. [CrossRef]
22. Wang, F.J. *Computational Fluid Dynamics Analysis: CFD Software Principles and Applications*; Tsinghua University Press: Beijing, China, 2004.
23. Ding, T.; Cao, S.; Xue, X.; Ding, S.; Zhou, L.; Qiao, B. Simulation and experiment on single-channel and double-channel airflow field of orchard sprayer. *Trans. Chin. Soc. Agric. Eng.* **2016**, *32*, 62–68.
24. Li, Z.D.; Yang, W.C.; Zhang, T.; Wang, W.W.; Zhang, S.; Chen, L.Q. Design and suction performance test of sucking-seed plate combined with groove-tooth structure on high-speed precision metering device of rapeseed. *Trans. Chin. Soc. Agric. Mach.* **2019**, *35*, 12–22.
25. Li, Z.D.; He, S.; Zhong, J.Y.; Han, J.F.; Chen, Y.X.; Song, Y. Parameter optimization and experiment of the disturbance air-suction hole metering device for rapeseed. *Trans. Chin. Soc. Agric. Mach.* **2021**, *37*, 1–11.
26. *GB/T 9478-2005*; Grain Drill Test Method. National Standardization Administration of the General Administration of Quality Supervision, Inspection and Quarantine of the People's Republic of China: Beijing, China, 2005.